NANO LETTERS

2007
Vol. 7, No. 3
596−601

Intracellular Distribution of TiO_2–DNA Oligonucleotide Nanoconjugates Directed to Nucleolus and Mitochondria Indicates Sequence Specificity

Tatjana Paunesku,[†,‡] Stefan Vogt,[§] Barry Lai,[§] Jörg Maser,[§] Nataša Stojićević,[†] Kenneth T. Thurn,[†] Clodia Osipo,[||] Hong Liu,[‡] Daniel Legnini,[§] Zhou Wang,[⊥] Chung Lee,[#] and Gayle E. Woloschak*[,†,‡,▽,○]

Department of Radiation Oncology, Northwestern University, Chicago, Illinois 60611, Robert H. Lurie Comprehensive Cancer Center, Northwestern University, Chicago, Illinois 60611, X-ray Science Division, Advanced Photon Source, Argonne National Laboratory, Argonne, Illinois 60439, Cardinal Bernadin Cancer Center, Loyola University Medical Center, Maywood, Illinois 60153, Department of Urology, University of Pennsylvania Medical Center, Pittsburgh, Pennsylvania 15213, Department of Urology, Northwestern University, Chicago, Illinois 60611, Department of Radiology, Northwestern University, Chicago, Illinois 60611, and Department of Cell and Molecular Biology, Northwestern University, Chicago, Illinois 60611

Received October 20, 2006; Revised Manuscript Received December 18, 2006

ABSTRACT

Deoxyribonucleic acid (DNA) oligonucleotides hybridize to matching DNA sequences in cells, as established in the literature, depending on active transcription of the target sequence and local molarity of the oligonucleotide. We investigated the intracellular distribution of nanoconjugates composed of DNA oligonucleotides attached to TiO_2 nanoparticles, thus creating a locally increased concentration of the oligonucleotide. Two types of nanoconjugates, with oligonucleotides matching mitochondrial or nucleolar DNA, were specifically retained in mitochondria or nucleoli.

The use of free nucleic acids as therapeutic agents was conceptualized at the same time when the first attempts in genetic engineering were successfully concluded. Notwithstanding the difficulties regarding cellular uptake and intracellular stability of nucleic acids, oligonucleotides were found to be capable of "finding" the matching genomic sequence and leading to the repair of the target sequence.[1−4] The formation of matching hybrids inside cells is modulated by processes of transcription and replication.

Our interest lies in using a similar approach in order to develop an agent that can be triggered to cause not genomic DNA repair but the opposite, DNA damage extensive enough to cause gene inactivation. For this purpose, we are developing TiO_2 nanoparticles (3−5 nm) conjugated to one−five single-stranded DNA oligonucleotides (6−8 nm) via dopamine used as a bidentate enediol ligand for TiO_2.[5] The semiconductor TiO_2 nanoparticles can be excited, causing the electropositive holes to be injected into the DNA, ultimately leading to DNA scission as we have shown in vitro.[5,6]

The first step in developing nanoparticles for intracellular DNA targeting is to ensure that they have the capacity to be taken up by cells and retained at their target DNA sequence. Because it is very difficult to identify the precise position of a single gene DNA target inside cells, we decided to monitor targeting of genes located in specific subcellular compartments. Two such DNA targets with clearly defined subcellular locations are genes for ribosomal RNA (rDNA) located in the nucleolus inside the cell nucleus, and mitochondrial genes, located in mitochondria in cellular cytoplasm. Therefore, we decided to compare (1) oligonucleotide targeting the ribosomal 18S RNA gene located on the satellite

* Corresponding author. E-mail: g-woloschak@northwestern.edu.
[†] Department of Radiation Oncology, Northwestern University.
[‡] Robert H. Lurie Comprehensive Cancer Center, Northwestern University.
[§] X-ray Science Division, Advanced Photon Source, Argonne National Laboratory.
[||] Cardinal Bernadin Cancer Center, Loyola University Medical Center.
[⊥] Department of Urology, University of Pennsylvania Medical Center.
[#] Department of Urology, Northwestern University.
[▽] Department of Radiology, Northwestern University.
[○] Department of Cell and Molecular Biology, Northwestern University.

10.1021/nl0624723 CCC: $37.00 © 2007 American Chemical Society
Published on Web 02/03/2007

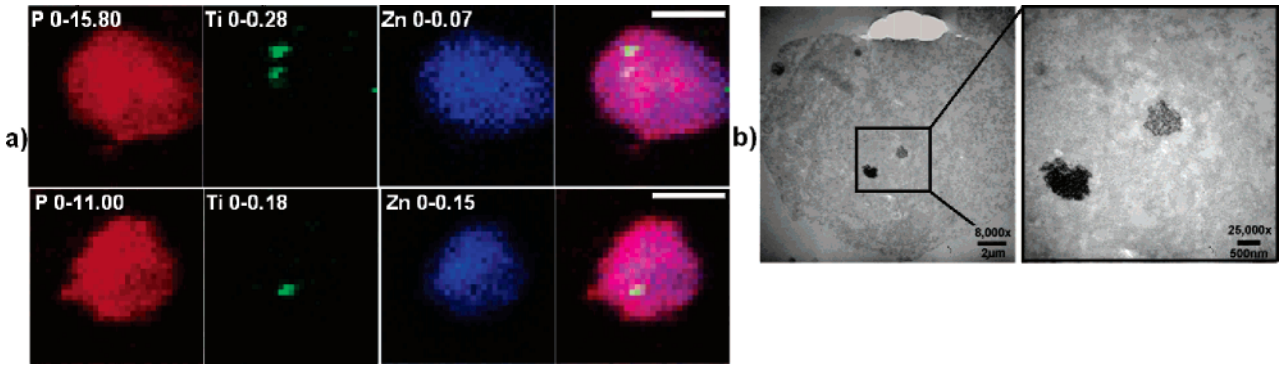

Figure 1. XFM maps and TM images of MCF7/WS8 cells transfected with nucleolus-specific nanoconjugates. (a) MCF7/WS8 cells were electroporated and imaged by X-ray fluorescence microscopy. Elemental maps and map overlaps are shown for P, Ti, and Zn. Scanning was done at 2ID-E beamline at the APS. White size bars are 10 μm. Numbers following elemental sign show elemental concentration in μg per cm^2. (b) TEM image of 100 nm thin section of a MCF7/WS8 cells electroporated with nucleolus specific nanoconjugate; left panel, cell cross section; right panel, TEM detail with two nanoconjugate rich spots. Imaging was done at Northwestern University Cell Imaging Core Facility.

arms of chromosomes and dispersed in the area of nucleolus in the interphase nucleus, (2) oligonucleotide targeting the mitochondrial genomic sequence, NADH dehydrogenase subunit 2 gene (ND2), and (3) nanoparticles without attached oligonucleotide DNA. While the DNA-free nanoparticles have no target inside cells, nucleolar and mitochondrial nanoconjugates have a similar number of targets per cell, albeit distributed differently. Ribosomal 18S gene is present in the genome in about 300 hundred copies[7] co-localized in one location, in nucleoli. The mitochondrial target is present in a few copies in each mitochondrion; because the majority of cells have several hundred mitochondria,[8] this target sequence has a similar frequency to the nucleolar target sequence, yet this target is interspersed throughout the cytoplasm.

For the experiments described here, TiO_2−DNA nanoconjugates were prepared fresh as described.[5] A colloidal nanoparticle solution with approximately 10 μM nanoparticle concentration was conjugated to dopamine-modified oligonucleotides. Nanoconjugates were prepared so that, on the surface of each nanoparticle, otherwise covered with glycidyl isopropyl ether, 1−5 dopamine-modified DNA molecules were attached. Sequences of the oligonucleotides attached to the nanoparticles were: (1) specific for the sense strand sequence of the NADH dehydrogenase 2 (ND2) mitochondrial gene present in the PC12 cell line: 5′ carboxy dT-cacgacaccttagcaccaacttac (ND2s); or (2) matching the sense stand of the R18S ribosomal RNA gene: 5′ carboxy dT-ttccttggatgtggt (R18Ss) universally present in mammalian cells. Sense strand oligonucleotides were chosen for these experiments in order to avoid hybridization with the RNA products of the two genes. The nanoparticles are coated with glycidyl isopropyl ether, which reduces their surface reactivity with the vast majority of chemical groups, making them nonreactive with most biological molecules. Therefore, oligonucleotide-free nanoparticles showed little retention inside cells at the 24 h post-transfection time point, while nanoconjugates with oligonucleotides remained inside cells (Figures 1−6).

We transfected human breast cancer cell line MCF-7/WS8 with nanocomposites specific for nucleolar target sequence (Figure 1). The cells were grown according to the instructions recommended by American Type Culture Collection (ATCC) to 80% confluence and at that time serum starved (incubated in serum free medium) for 16 h. Transfection was done by electroporation: $1-3 \times 10^6$ cells were electroporated with 5−15 μL of 10 μM nanoconjugate solution (with 2−6 oligonucleotides per particle) using the Mammozapper apparatus (Tritech, Carlsbad, CA) following the manufacturer's instructions. The electroporated cells were resuspended in 8 mL of complete medium and allowed to attach to the tissue culture dishes for 2 h; at that time, cells were washed free of excess nanoconjugates: medium was removed, cells were rinsed with the new complete medium, and then 10 mL of the fresh medium was added to cells for an additional 24 h. At the end of this time, cells were harvested for imaging.

Because these nanoconjugates cannot be visualized by optical microscope, we used two alternative approaches to determine their localization. One technique available to us was transmission electron microscopy. Ultrathin (100 nm) sections of transfected cells embedded in epoxy resin were cut with a diamond knife onto 200 mesh nickel grids, stained with osmium tetraoxide, uranyl acetate, and lead citrate. Analyses of cell sections were performed in a transmission electron microscope (JEOL 1220, JEOL USA, MA). Imaging was done at Northwestern University Cell Imaging Core Facility. The density of TiO_2 surpasses the density of cellular material, and we were able to determine the presence of TiO_2 in two regions ~0.5 μm inside the nuclei of nanoconjugate treated cells. At the same time, no such "denser" material was found in mitochondria of these cells.

A more direct approach to image titanium itself is to detect it by Kα characteristic X-ray fluorescence using X-ray fluorescence microscopy (XFM). This technique allows simultaneous mapping of chemical elements by their Kα specific fluorescence. The XFM facility we used at the 2ID-E and 2ID-D beamlines at the Advanced Photon Source at Argonne National Laboratory is best equipped for mapping

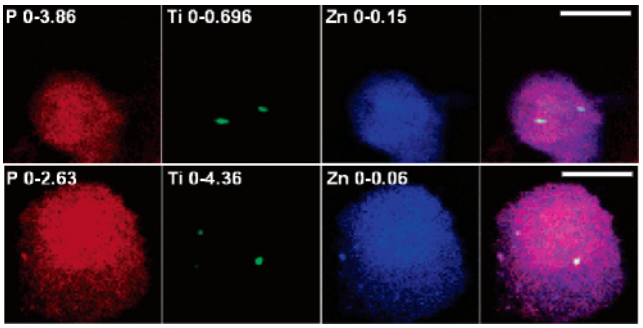

Figure 2. XFM maps of whole PC3 cells transfected with nucleolus-specific nanoconjugates. Top row, electroporation; bottom row, natural uptake. In both cases, elemental maps and map overlaps are shown for P, Ti, and Zn. Scanning was done at 2ID-E beamline at the APS. White size bars are 10 μm. Numbers following elemental sign show elemental concentration in μg per cm^2.

of elements between Si and Zn in the periodic table. An undulator source was used to generate hard X-rays with energy of 10 keV. A single-bounce Si ⟨111⟩ monochromator was used to monochromatize the X-rays; they were then focused to a beam spot ~0.4 μm × 0.3 μm in size using Fresnel zone plate optics with a focal length of 25 cm (Xradia, Concord, CA) at the 2ID-E beamline, or a beam spot ~0.3 μm × 0.2 μm formed by a Fresnel zone plate with a focal length of 12.9 cm is produced at the 2ID−D beamline. Characteristic X-ray induced X-ray fluorescence was detected using an ultra-LEGe energy dispersive detector (Canberra, Meriden, CT). Elemental maps were built point by point, raster-scanning the sample by moving it through the focal spot. The fluorescence spectra were acquired at every specimen position and were fitted with modified Gaussians corresponding to X-ray fluorescence lines. Quantification was done by comparison of normalized fluorescence counts from the sample to NBS thin film standards 1832 and 1833 (NIST, Gaithersburg, MD). Elemental quantification and co-localization of elemental signals was investigated using the MAPS program.[9]

The XFM technique is used for imaging of whole cells, which enables one to determine the total elemental content in the complete volume of the desired region of interest. P, Ti, and Zn elemental maps were acquired simultaneously; the presence of P and Zn signals indicates the outline of the cells while the "internal" more intense P and Zn signals suggest the area of the nucleus. The pattern of spots indicates the presence of Ti (and therefore nanoconjugates) in the nuclei.

To ensure that these results are not unique to MCF-7/WS8 cells, we investigated transfection of other cell types: PC3 human prostate cell line (Figure 2) and rat pheochromocytoma cell line PC12 (data not shown). Moreover, we used different approaches for transfection, comparing their results to the results obtained by electroporation. Transfection by electroporation can be considered as a "gold standard"

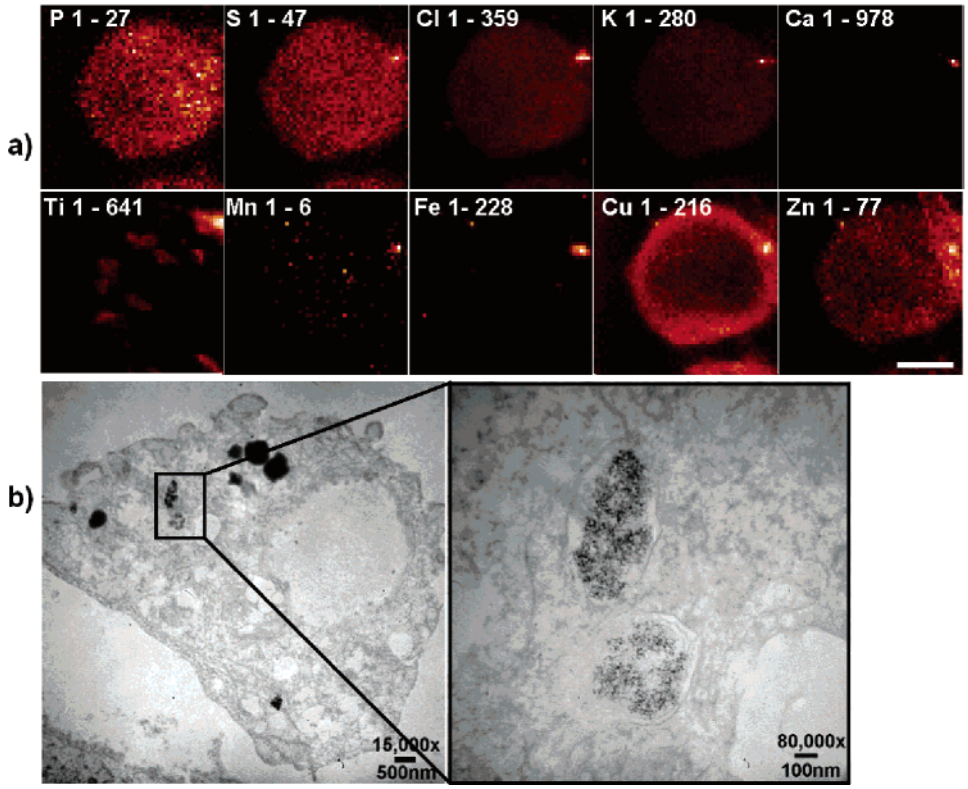

Figure 3. XFM and TEM images of PC12 cells electroporated with mitochondria-specific TiO_2−DNA nanoconjugates. (a) XFM maps for P, S, Cl, K, Ca, Ti, Mn, Fe, Cu, and Zn of a whole PC12 cell electroporated by a mitochondria-specific nanoconjugate. Elements are indicated inside each map. Elemental concentrations are given as relative signal intensity. Size bar is 5 μm. (b) TEM image of a 100 nm thin section of a PC12 cell electroporated by a mitochondria specific nanoconjugate. Left: cell with several mitochondria containing nanoconjugate. Right: detailed image of two adjacent mitochondria. The very dense nongranular material located in the cell vacuoles is osmium tetraoxide.

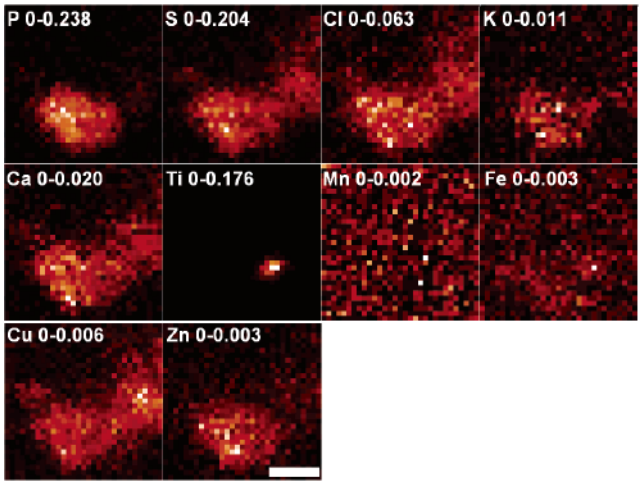

Figure 4. XFM map of isolated mitochondria of PC12 cells electroporated with mitochondria-specific (NADH dehydrogenase 2 specific) nanoconjugates. Elemental maps of P, S, Cl, K, Ca, Ti, Mn, Fe, Cu, and Zn were done for mitochondria isolated from PC12 cells electroporated with nanoconjugates carrying ND2s oligonucleotide and then "washed" for 24 h in nanoconjugate-free medium. Elemental maps show the range of concentrations in the sample in a "red temperature scale" from highest (white) to lowest (black) signal. The scan area was 3 μm × 3 μm, with a step size of 0.1 μm. Scanning was done at 2ID-D beamline at the APS. Elemental concentrations are shown in μg per cm^2. Size bar is 1 μm.

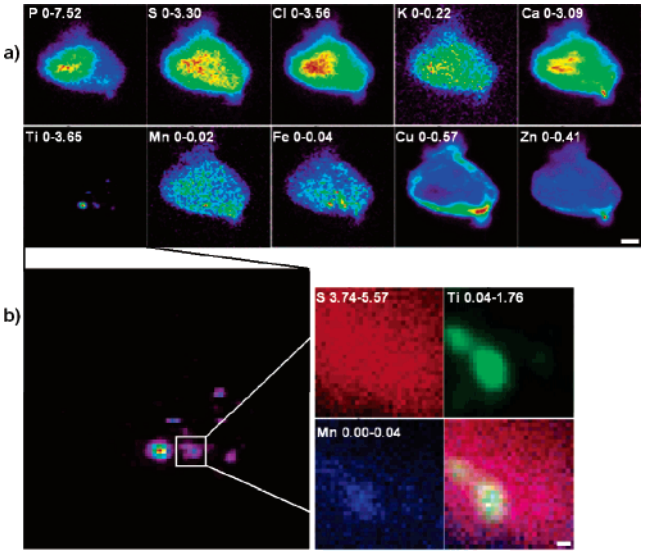

Figure 5. XFM maps of whole PC12 cell transfected with mitochondria-specific nanoconjugates using natural uptake. (a) Elemental maps of P, S, Cl, K, Ca, Ti, Mn, Fe, Cu, and Zn in PC12 cell treated with nanoconjugates carrying ND2s oligonucleotide for 24 h and then "washed" for 24 h in nanoconjugate-free medium. Elemental maps show the range of concentrations in the sample in a rainbow color scale from highest (red) to lowest (black) signal. Scan area was 13 μm × 12.8 μm, with 0.2 μm step. Scanning was done at 2ID-D beamline at the APS. Elemental concentrations are given in μg per cm^2. White size bar is 2 μm. (b) Enlarged Ti maps of the cells in (a) and a detailed XFM map of a mitochondria inside the cell. Left: enlarged Ti map of the whole cell from the right panel of Figure 3a. Right: S, Ti, Mn and overlap maps for the mitochondria-shaped form from the left panel. The scan area was 1.5 μm × 1.5 μm with 50 nm step. Scanning was done at 2ID-D beamline at the APS. White size bar is 100 nm.

approach because it delivers the transfection material equally in every subcellular compartment. It is therefore retention of nanoconjugates that dictates their location in cells at 24 h post transfection. We were able to observe nanoconjugate retention in cells of different origins because we were using the nucleolar nanoconjugate with a universal probe sequence that targets rRNA 18S genes in most mammalian species. Cancer cells most often contain two or more nucleoli; in these cells, the Ti signal was often found to look like a pair of spots (Figure 1 and 2). XFM elemental maps of prostate cancer PC3 cells (Figure 2), same as breast cancer MCF7/WS8 cells (Figure 1) and pheochromocytoma cells (data not shown) showed in most cases a two-spot pattern. This type of pattern was, moreover, present both in electroporated cells (Figures 1, 2, top) and cells that were transfected by nanoconjugates by natural uptake (Figure 2, bottom).

To address the capacity of nanoconjugates to be retained inside mitochondria, we used a mitochondrial nanoconjugate specific for NADH dehydrogenase 2 to transfect rat pheochromocytoma cell line PC12 by electroporation (Figures 3 and 4) or natural uptake (Figure 5).

PC12 cells electroporated by mitochondria specific nanoconjugate were imaged both by XFM mapping and by transmission electron microscopy (Figure 3). In the TEM images of these cells, we found no granular material in the nuclei. Mitochondria, on the other hand, contained denser granular material resembling the nanoparticles.

In addition to imaging of whole cells and cell sections, we used electroporated PC12 cells as a source from which we have isolated free mitochondria. In this case, sectioning of the cell was not necessary to show the presence of nanoconjugates inside mitochondria. Isolated mitohondria were imaged by XFM (Figure 4), showing presence of titanium.

In addition to electroporation, we transfected PC12 cells with mitochondria specific nanoconjugates by natural uptake. We could not test the retention of this nanoconjugate in non-rat cell lines because oligonucleotides probe−ND2s oligonucleotide matches only the rat mitochondrial genomic sequence. Following a 24 h wash, we imaged PC12 cells transfected by mitochondrial nanoconjugate by XFM (Figure 5a). A detailed image of the region likely containing a mitochondrion is shown in Figure 5b. The more intense Mn signal outlines the mitochondria in Figure 5b due to the increased presence of this metal in the mitochondrial matrix, bound to mitochondrial manganese superoxide dismutase protein.

Figure 6 shows a correlation between the specific types of the nanoconjugates used: free TiO_2 nanoparticle (without DNA attached), nucleolar nanoconjugate and mitochondrial nanoconjugate, and ratio of Ti to Zn in these cells. We used cluster analysis to define cells as regions of interest, calculated elemental content for P, S, Ca, Zn, and Ti within the cells, and calculated, for P, S, Ca, and Ti, the average normalized elemental content using Zn quantity for normalization. Zn is present in all cells, co-localized with cellular material, and therefore, completely overlaps with other

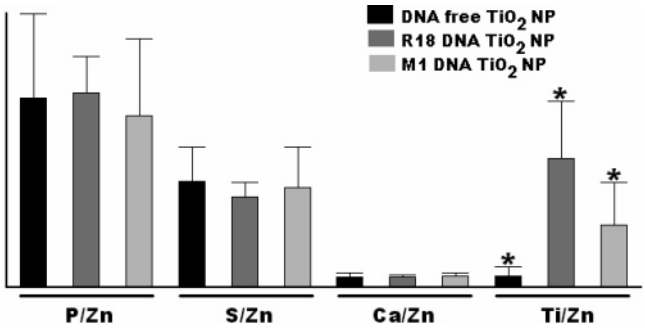

Figure 6. Ratios of intracellular concentrations of P, S, Ca, and Ti compared to Zn when different nanoparticles/nanoconjugates are used. Each type of nanoparticle/ nanoconjugate transfection was indicated by different colors: DNA-free TiO_2 nanoparticles (DNA free TiO_2 NP) (black), nanoconjugates specific for nucleolar rDNA (R18 DNA TiO_2 NP) (dark gray), and nanoconjugates specific for mitochondrial DNA (M1 DNA TiO_2 NP) (light gray). Elemental ratios for each group of three sample preparations were shown together as indicated below the graph. Average ratios were derived from several scans (15 for free nanoparticle, seven for ribosomal rDNA, and nine for mitochondrial DNA) and shown as bar graphics, with the standard deviation shown as overlaid error bars. Samples showing statistically significant variation are indicated by asterisks.

natural cellular elements such as P, S, and Ca. Because of that, ratios of the elemental concentrations of P/Zn, S/Zn, and Ca/Zn were the same in all three groups of samples. However, the variation between the ratios of Ti/Zn among the three groups of cells transfected with three types of nanoconjugates was statistically significant (Figure 6, Supporting Information Table 1). This statistical analysis was done using GraphPad InStat3 software version 3.06 (GraphPad, San Diego, California). A nonparametric ANOVA test, Kruskal−Wallis Statistic was used; Dunn's Multiple Comparison Test was used to evaluate probability of statistical significance of mean rank difference between samples.

In conclusion, in our experiments different nanoconjugates were retained in detectable quantity only in those subcellular compartments for which the nanoconjugates were designed: nucleolar nanoconjugates inside nuclei and mitochondrial nanoconjugates in mitochondria. In each experiment, the absence of the tested nanoconjugate from the nontargeted subcellular compartment served as a negative control. Mitochondrial and nucleolar nanoconjugates differed only in the nucleotide sequence of their DNA oligonucleotides, and no other aspect of the nanoconjugate synthesis; the nanoparticles came from the same pool of nanoparticles, both oligonucleotides were attached to the dopamine at the same time and using the same technique and subsequently mixed with the nanoparticles in order to create the final nanoconjugates. Therefore, sequence-specific retention of the nanoconjugates is based on the ability of the oligonucleotide component of the nanoconjugate to establish a DNA hybrid with the complementary intracellular sequence. The high rate of transcription in both mitochondria and nucleoli is probably one of the deciding factors that made these results possible.

The uptake of nanoconjugates by all three methods tested resulted in presence of nanoconjugates inside cells; therefore it appears that the TiO_2 bound oligonucleotides behave similarly to oligonucleotides alone. Natural uptake of DNA can be either enocytosis or receptor mediated, depending on the concentration of DNA.[10] In both cases, a certain amount of transfected DNA does end up inside the nucleus. Uptake of DNA by mitochondria was also detected in those experiments where electroporation was used as a means for transfection.[11]

The number and uses of bionanoconjugates are growing daily. Medical imaging techniques (encompassing detection, identification, and diagnostics), therapeutics, and basic science are all beginning to benefit from the use of nanoscale materials such as metal and metal oxide nanoparticles, nanowires, and quantum dots,[12−17] reaching such new ground as in vivo imaging,[18,19] delivery of drug payloads,[12,14] and have long since begun to improve photodynamic and heat therapy.[20,21]

Nanoconjugates with oligonucleotide components exist in several guises, with nanoparticles made of different materials.[5,12,13,15,16,22] Functions of these nanoconjugates are varied as well, from imaging[17,18,21] to nucleic acid, DNA,[5] or RNA[13] hybridization and/or cleavage, with or without aid from the cellular enzymatic machinery. In this work, we determined sequence specificity of the subcellular retention of TiO_2−DNA nanoconjugates, suggesting that it is possible to use the TiO_2−DNA nanoconjugates for sequence specific local treatment of DNA targets.

Acknowledgment. This work was supported by NIH CA107467, EB002100, P50 CA89018, U54CA119341, and by DOE FG02−04 ER 63920. TiO_2 nanoparticles used for some of these studies were a gift from T. Rajh and M. Thurnauer (Chemistry Division, Argonne National Laboratory, Argonne, IL). TEM was done at the Northwestern University Cell Imaging Facility, and we are grateful to Lennell Reynolds for his help with sample preparation and TEM imaging. XFM experiments were performed at 2ID-E and D beamlines of the X-ray Operations and Research, Advanced Photon Source, Argonne National Laboratory. Use of the Advanced Photon Source was supported by the U.S. Department of Energy, Office of Science, Office of Basic Energy Sciences, under contract no. W-31-109-Eng-38.

Supporting Information Available: Table showing probability of statistical significance variation between median values, Kruskal−Wallis statistic, and probability of statistical significance of mean ranks difference by Dunn's Multiple comparison test done for pairs. This material is available free of charge via the Internet at http://pubs.acs.org.

References

(1) Kren, B. T.; Chen, Z.; Felsheim, R.; Roy Chowdhury, N.; Roy Chowdhury, J.; Steer, C. J. *Gene Ther.* **2002**, *9*, 686−690.
(2) Andersen, M. S.; Sorensen, C. B.; Bolund, L.; Jensen, T. G. *J. Mol. Med.* **2002**, *80*, 770−781.
(3) Igoucheva, O.; Alexeev, V.; Yoon, K. *Gene Ther.* **2001**, *8*, 391−399.
(4) Liu, L.; Rice, M. C.; Kmiec, E. B. *Nucleic Acids Res.* **2001**, *29*, 4238−4250.
(5) Paunesku, T.; Rajh, T.; Wiederrecht, G.; Maser, J.; Vogt, S.; Stojićević, N.; Protić, M.; Lai, B.; Oryhon, J.; Thurnauer, M.; Woloschak, G. *Nat. Mater.* **2003**, *2*, 343−346.
(6) Paunesku, T.; Sojicevic, N.; Vogt, S.; Maser, J.; Lai, B.; Rajh, T.; Thurnauer, M.; Woloschak, G. *J. Phys. IV* **2003**, *104*, 317−319.

(7) Makalowski, W. *Acta Biochim. Pol.* **2001**, *48*, 587−598.
(8) Allard, C.; De Lamirande, G.; Cantero, A. *Cancer Res.* **1952**, *12*, 580−583.
(9) Vogt, S.; Maser, J.; Jacobsen, C. *J. Phys. IV* **2003**, *104*, 617−622.
(10) de Diesbach, P.; N'Kuli, F.; Berens, C.; Sonveaux, E.; Monsigny, M.; Roche, A-C.; Courtoy, P.J. *Nucleic Acids Res.* **2002**, *30*, 1512−1521.
(11) McGregor, A.; Temperley, R.; Chrzanowska-Lightowlers, Z. M.; Lightowlers, R. N. *Mol. Genet. Genomics* **2001**, *265*, 721−729.
(12) Ferrari, M. *Curr. Opin. Chem. Biol.* **2005**, *9*, 343−346.
(13) Rosi, N. L.; Giljohann, D. A.; Thaxton, C. S.; Lytton-Jean, A. K. R.; Han, M. S.; Mirkin, C. A. *Science* **2006**, *312*, 1027−1030.
(14) Ferrari, M. *Nat. Rev. Cancer* **2005**, *5*, 161−171.
(15) Bruchez, M., Jr.; Moronne, M.; Gin, P.; Weiss, S.; Alivisatos, A. P. *Science* **1998**, *281*, 2013−2016.
(16) Cao, Y. C.; Jin, R.; Mirkin, C. A. *Science* **2002**, *297*, 1536−1540.
(17) Park, S. J.; Taton, T. A.; Mirkin, C. A. *Science* **2002**, *295*, 1503−1506.
(18) Winter, P. M.; Caruthers, S. D.; Kassner, A.; Harris, T. D.; Chinen, L. K.; Allen, J. S.; Lacy, E. K.; Zhang, H.; Robertson, J. D.; Wickline, S. A.; Lanza, G. M. *Cancer Res.* **2003**, *63*, 5838−5843.
(19) Smith, A. M.; Gao, X.; Nie, S. *Photochem. Photobiol.* **2004**, *80*, 377−385.
(20) Allemann, E.; Rousseau, J.; Brasseur, N.; Kudrevich, S. V.; Lewish, K.; van Lier, J. E. *Int. J. Cancer* **1996**, *66*, 821−824.
(21) Ito, A.; Shinkai, M.; Honda, H.; Kobayashi, T. *Cancer Gene Ther.* **2001**, *8*, 649−654.
(22) Fu, A. H.; Micheel, C. M.; Cha, J.; Chang, H.; Yang, H.; Alivisatos, A. P. *J. Am. Chem. Soc.* **2004**, *126*, 10832−10833.

NL0624723